Nanoscale

Accepted Manuscript

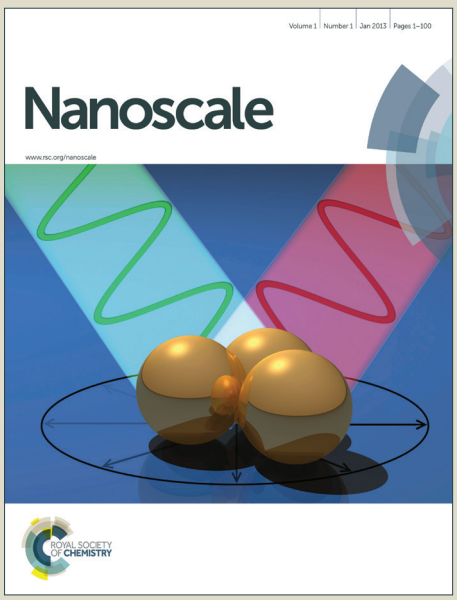

ROYAL SOCIETY OF CHEMISTRY

www.rsc.org/nanoscale

Nanoscale

RSCPublishing

ARTICLE

Non-linear optical properties of gold quantum clusters. The smaller the better.

Cite this: DOI: 10.1039/x0xx00000x

Isabelle Russier-Antoine, Franck Bertorelle, Marin Vojkovic, Driss Rayane, Estelle Salmon, Christian Jonin, Philippe Dugourd, Rodolphe Antoine* and Pierre-François Brevet

Received 00th January 2012,
Accepted 00th January 2012

DOI: 10.1039/x0xx00000x

www.rsc.org/

By developing a new method for synthesizing atomically monodisperse Au_{15} nanoclusters stabilized with glutathione molecules and using the current state-of-the-art methods for synthesizing monodisperse protected Au_{25} nanoclusters, we investigate their nonlinear optical (NLO) properties after two-photon absorption. The two-photon emission spectra and the first hyper-polarizabilities of these particles were obtained using, in particular, hyper-Rayleigh scattering technique. The influence on NLO of the excitation wavelength, the size as well as the nature of the ligands are also explored and discussed. Au_{15}, the *smallest* stable thiolated gold nanocluster, presents remarkable nonlinear properties with respect to two-photon processes. The TPA cross section at 780 nm for Au_{15} is ~ 65700 GM. This experimental cross-section value points to a quantum yield for two-photon emission of about $3x10^{-7}$ at 475 nm for Au_{15}. The first hyperpolarizability β for Au_{15} clusters (509×10^{-30} esu), as compared to Au_{25} clusters (128×10^{-30} esu) is larger considering the difference in the number of gold atoms. Also, the 10^{30}.β/atom values reported for Au_{15} and Au_{25} clusters are more than two orders of magnitude larger than the values reported for Au NPs in the size range 10-50 nm, outlining the quantum cluster regime.

Introduction

Due to discrete energy levels and molecular-like HOMO-LUMO transitions, ultrasmall clusters exhibit a spectacular optical behavior which is fundamentally different from that of larger plasmonic nanocrystals.[1] Recently, considerable progress has been achieved in the study of the linear and nonlinear optical properties of gold nanoparticles and clusters of varying size and shape.[2-4] The evolution of nonlinear optical properties, from gold atomic clusters to plasmonic nanocrystals has been addressed by Thomas and co-workers.[5] In particular they showed that the third-order optical nonlinearity in these ultrasmall gold clusters exhibits a significantly lower threshold for optical power limiting. On the other hand, the relatively strong emission under single-photon excitation for Au clusters leads to questions about the possibility of two-photon excited emission. For instance, by measuring two-photon fluorescence excited at 800 nm, Goodson et al.[6] have shown that two-photon absorption (TPA) cross-section increases as the size of small gold clusters increases from 1.1 to 4.0 nm. The TPA cross-section for Au_{25} is 427 000 GM, much larger compared to a typical value of approximately 1 000 GM at 800 nm for organic macromolecules. The large TPA cross sections open the way for applications of such small clusters in optical power limiting, nanolithography, and multiphoton biological imaging. Concerning biological imaging, recent developments in optical imaging techniques, in particular multi-photon excitation microscopy that allows studies of biological interactions at a deep cellular level, has motivated intensive research in developing multi-photon absorption fluorophores. For example, Polavarapu et al.[7] successfully demonstrated the applications of water soluble glutathione small gold clusters for both one and two-photon excitation live cell imaging.

Nonlinear optical (NLO) microscopies (two photon microscopy, TPM or second harmonic imaging microscopy, SHIM) received a tremendous interest for 3D imaging of biological tissues.[8] TPM and SHIM are based on fundamentally different NLO processes, two-photon excited fluorescence (TPEF) and second harmonic generation (SHG), respectively. Therefore, they provide complementary information and can be implemented simultaneously in the same microscope.[9] Whereas TPEF labels give information about molecular distribution, the coherent SHG signal is sensitive to the local non-centrosymmetric organization of the dye molecules and find promising applications for example for the measurement of membrane potential of the neuronal activity of the brain.[10, 11]

While numerous works were devoted to measure the TPA cross-sections of low nuclearity Au clusters,[4] their non-linear susceptibilities were only scarcely explored. Third-order nonlinear optical susceptibilities of monolayer-protected Au_{25} were recently reported[5, 12] as well as the one for Au_{15} in contact with indium tin oxide films.[13] The first hyper-polarizabilities of silver quantum clusters of different sizes (Ag_{20}, Ag_{140} and Ag_{980}) have been recently measured using hyper-Rayleigh scattering technique.[14] In this paper, we aim at exploring NLO properties of ultra-small gold clusters protected by various functionalized thiols. Based on the current state-of-the-art methods for synthesizing atomically monodisperse protected Au_{25} nanoclusters,[15, 16] and reporting a new method for synthesizing atomically monodisperse Au_{15} nanoclusters stabilized with glutathione molecules, we report the TPE spectra and their first hyper-polarizabilities using hyper-Rayleigh scattering technique. The influence on NLO of the excitation wavelength (between 780 and 900 nm), the size (Au_{15} vs Au_{25}) and the nature of the ligands (glutathione vs cysteine) is also explored and discussed.

Results and discussion

Characterization and linear optical properties of as-prepared protected gold clusters. The gold clusters produced by synthesis described in supporting information (see methods section and fig. S1) were characterized by mass spectrometry and optical methods. The monodispersity in term of the size of the prepared gold clusters was verified by ESI-mass spectrometry. An ESI mass spectrum for the protected Au_{15} cluster from solution, and acquired under gentle ESI conditions is shown in Figure 1a). A charge state distribution was observed from $[M-4H^+]^{4-}$ through $[M-8H^+]^{8-}$. Deconvolution of charge states 4− through 8−, and using a multiplicative correlation algorithm,[17, 18] provided a mass of 6928 Da for the intact Au cluster, consistent with the calculated mass of $Au_{15}SG_{13}$ (see inset Fig. 1a). Also, PAGE for Au:SG clusters using Tsukuda synthesis[19, 20] and for our synthesis confirms the monodispersity in term of the size of the prepared $Au_{15}SG_{13}$ clusters (see inset Fig. 1b). Fig. 1b shows the UV-vis absorption spectra in solution of the synthesized $Au_{15}SG_{13}$ clusters. The main feature of the spectrum is a monotonic increase in the electron absorption as the laser wavelength decreases with an onset at ~500 nm and a shoulder observed at ~400 nm. The strong absorption arises from mixed intraband (sp←sp) and interband (sp←d) transitions.[21] Fig. 2c displays the photoemission and photoexcitation spectra of $Au_{15}SG_{13}$. An emission band centered at ~800 nm is observed and originates from radiative intraband transitions within the sp bands across the HOMO-LUMO gap.[19, 20] The excitation spectrum traces well the profiles of the corresponding absorption spectra (see Fig. 1b and 1c), indicating that the sp intraband excitations are responsible for the photoemission. For comparison, Figs. S2 and S3 show the optical absorption spectra of aqueous solutions of $Au_{25}SG_{18}$ and $Au_{25}Cys_{18}$ as well as the corresponding ESI

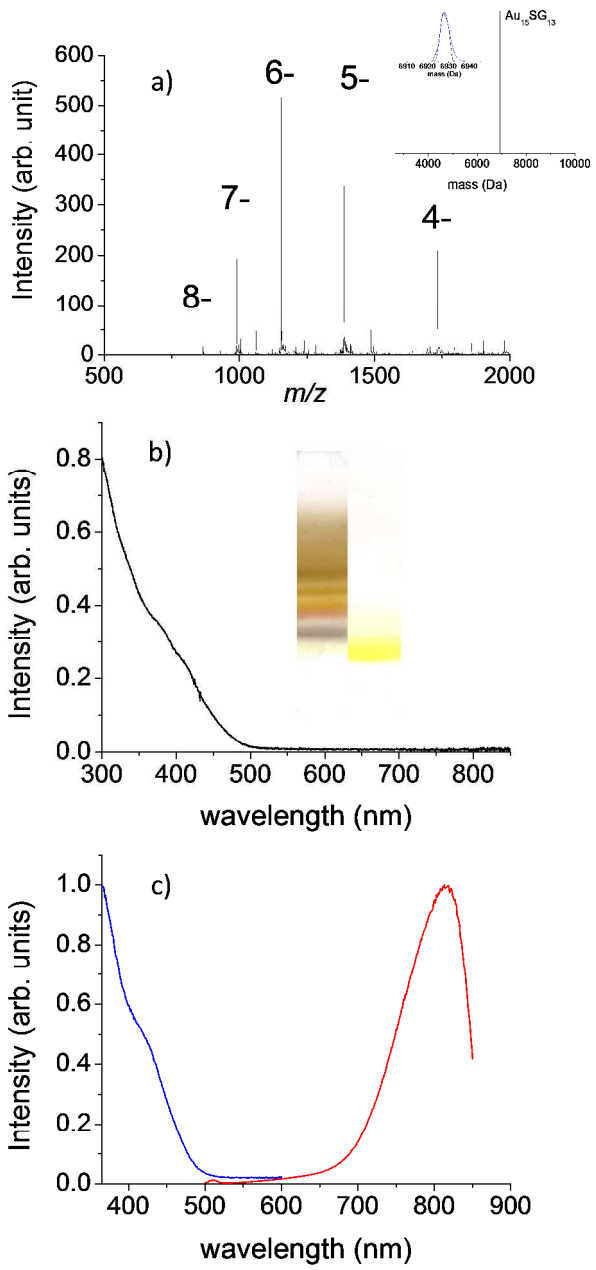

Figure 1 : (a) ESI mass spectrum for the protected Au15 cluster from water solution, and acquired under gentle ESI conditions. Inset. ESI deconvoluted spectrum of $Au_{15}SG_{13}$, based on the experimental ESI spectrum and using a multiplicative correlation algorithm. Comparison of the experimental and simulated deconvoluted spectra of $Au_{15}SG_{13}$. (b) (Black line) Absorption spectrum of $Au_{15}SG_{13}$. Inset: PAGE for Au:SG clusters using (left) Tsukuda synthesis (see ref. 19) and (right) our synthesis. (c) Photoexcitation (with an emission at 820 nm) and emission spectra (with an excitation at 435 nm) of $Au_{15}SG_{13}$.

spectra. The optical spectra are very similar to those reported in the literature.[15, 16, 19] The main features of the spectra are a monotonic decrease in the absorption as the laser wavelength increases and a broad band on the red side of the spectrum (around 650 nm). Both Au_{25} cluster (protected with glutathione and cysteine) solutions display the two features described

above. The absorption band on the red side of the spectrum is due to the intraband transition (HOMO−LUMO) derived from sp orbitals of Au[21, 22] and is systematically observed for protected Au_{25} clusters.[15, 19, 23, 24] The excitation spectra trace well the profiles of the corresponding absorption spectra and an emission band centered at ~800-850 nm is also observed. Optical spectra in solution are very similar to those reported by Tsukuda and coworkers[19, 20] on separated band after PAGE separation.

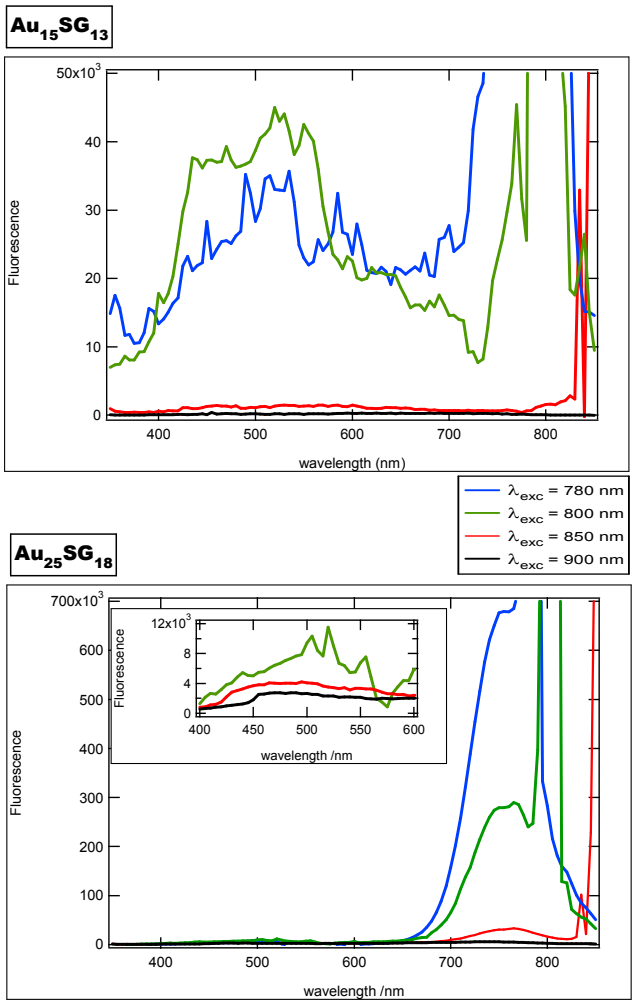

Figure 2: Two-photon emission spectra for $Au_{25}SG_{18}$, $Au_{15}SG_{13}$ as a function of wavelength for different excitation wavelengths (780, 800, 850 and 900 nm). The huge increases in the right part of the spectra are due to the excitation laser lines (780, 800, 850 and 900 nm).

Two-photon absorption and emission of as-prepared protected gold clusters. Two-photon excited fluorescence spectra with excitations ranging from 780 nm to 900 nm have been recorded for Au_{15} and Au_{25} gold clusters. Spectra are given in Fig. 2. A broad band in the visible range (between 400 and 600 nm) is observed and is more intense for Au_{15} clusters than for Au_{25} clusters. Fluorescence in the visible region was observed for gold nanoparticles and nanoclusters (in particular Au_{25}).[4, 6] Interestingly a well-defined intense band centered at ~750 nm appears for Au_{25} in the near IR region (between 700 nm and 800 nm) and is certainly due to the radiative intraband transitions within the sp bands across the HOMO-LUMO gap reported for protected Au_{25} clusters (see also Figs. S2 and S3).[19, 20] No absorption is observed in the red part of the spectrum for Au_{15} clusters (see Figure 1b) which is in agreement with a TPE spectrum dominated by a broad band between 400 nm and 600 nm.

We attempt to determine the two-photon cross-section at 475 nm of gold clusters. The number of fluorescence photons collected in an experiment is given by :[25]

$$F(t) = \frac{1}{2}\,\phi\eta_2 N(t) \qquad (1)$$

Where *N(t)* is the number of excited molecules, η_2 the quantum efficiency for fluorescence of the molecule and ϕ the collection efficiency of the experimental arrangement. The ½ factor accounts for the physical reduction by half of the number of photons owing to the two-photon excitation process.

For a pulsed excitation, the number of excited photons is :

$$N(t) = \sigma_2 C \frac{g_p \langle P(t)\rangle^2}{f\tau\pi\lambda/n} \qquad (2)$$

Where σ_2 is the two-photon absorption (TPA) cross-section, *C* the concentration, *f* the laser pulse frequency, τ the pulse duration, g_p its second-order coherence function, λ the excitation wavelength, *n* the optical index at that frequency and $\langle P(t)\rangle$ the incident power averaged over a duty cycle. Using Eqs.(1) and (2), it is experimentally simpler to compare the two-photon excited fluorescence of the sample and that of a known reference compound. Here, we have chosen fluorescein dye as an internal reference. From literature, we assume at the excitation wavelength of 780 nm : σ_2 (fluorescein) = 33.3 GM using a quantum yield of 0.9 and two photon absorption cross-section of 37 GM.[26] Fluorescein dye was used at the low concentration of 10 µM in order to obtain two-photon emission yields compatible with the Au_{15} and Au_{25} two-photon yields. In particular, no changes in the experimental settings were performed between the two measurements.

Experimentally, we find for the TPE fluorescence cross section at 475 nm: 0.022 GM for Au_{15} but only 0.0022 GM for Au_{25} clusters. As expected, for the same excitation wavelength, the TPE fluorescence cross section at 755 nm is only 0.82 GM whereas it is 4.99 GM for Au_{25}. Since this cross-section value is rather low, its power dependence with the square of the input laser intensity was checked. Fig. S4 in supporting information shows the fluorescence spectra obtained after excitation at 800 nm and at different pump-powers for Au_{15} and pump-power dependence of the fluorescence which gave a slope of ~2 suggesting also that it is indeed a two-photon excited emission. Interestingly, we also measured the TPA cross section at 780 nm for Au_{15} and we found σ (TPA, $Au_{15}SG_{13}$) = 65700 GM. Detailed TPA experimental arrangement, using a P-scan set-up

is given in supporting information (see Fig. S5). These experimental cross-section values point to a quantum yield (QY= $\sigma_{TPE}/\sigma_{TPA}$) for Au_{15} of about $3x10^{-7}$ at 475 nm, in very good agreement with what is expected for such compounds.[6]

Hyperpolarizability measurements. In these experiments where the HRS intensity is collected, the monochromaticity of the second harmonic light generated was always assessed to prevent any spurious contributions from fluorescence. To this end, the HRS intensity for different concentration was normalized against that of the bare solvent. At each concentration, a 20 nm narrow band spectrum around the HRS line was recorded, see Fig. 3. This experimental procedure is deemed necessary to ensure that the process indeed corresponds to the conversion of two photons at the fundamental frequency into one photon at the harmonic frequency. It is observed in particular that the HRS line is located on top of the strong fluorescence background. Two methods are known to remove this fluorescence background, a time-domain and a spectral-domain method. Here the spectral domain method was used owing to the experimental gated photon counting set-up used. The subtraction of the background was then performed by fitting the narrow band spectra with a Gaussian function for the HRS line superposed on a linear function of the wavelength accounting for the fluorescence background. This subtraction procedure is allowed since the two processes, fluorescence and HRS, are incoherent.

The HRS intensity is then given by :

$$\frac{I_{HRS}}{I_{HRS}^{w}} = \frac{\langle N_w\beta_w^2 + N\beta^2 \rangle}{\langle N_w\beta_w^2 \rangle} = 1 + b' N \langle \beta^2 \rangle \qquad (3)$$

where $b' = 1 / N_w \langle \beta_w^2 \rangle$ (4)

with the subscripts *w* standing for water, the reference solvent used in this experiment. The losses due to absorbance at the fundamental and the harmonic frequency were determined from the separate UV-visible absorption measurements and all data were corrected prior to the analysis. The HRS intensity recorded for different concentrations of $Au_{15}SG_{13}$ in aqueous solution is reported in Fig.3.

As seen in Eq.(3), it is necessary to know the hyperpolarizability of the bare solvent to determine the hyperpolarizability of the gold clusters. In the present report, we use the value of $0.087x10^{-30}$ esu for the first hyperpolarizability of the neat water solution. A discussion on this value may be found in a previous work.[27] The hyperpolarizability values obtained for the different solutions are reported in Table 1.

Interestingly $Au_{25}SG_{18}$ and $Au_{25}Cys_{18}$ have similar hyperpolarizability, meaning that the ligands size has only a weak effect on the SH generation. An absolute value of $(0.16 \pm 0.01) \times 10^{-30}$ esu for the first hyperpolarizability of nonaromatic amino acids was reported by Duboisset et al.[28] And by using a collagen like model, the microscopic hyperpolarizability along the peptide bond was evaluated at $(0.7 \pm 0.1) \times 10^{-30}$ esu. It is clear that the huge hyperpolarizabilities reported in this work cannot be accounted by the ligand shell alone (which only would give a contribution of several 10^{-30} esu for the first hyperpolarizability for a fully coherent superposition). The first hyperpolarizability for Au_{15} clusters, as compared to Au_{25} clusters is also larger considering the difference in the number of gold atoms. Structural theoretical investigations on $Au_{15}(SR)_{13}$ model features staple motifs protecting the Au_4 nucleus.[29, 30] On the other hand, the Au_{25} cluster features a centered icosahedral Au_{13} core capped by twelve gold atoms that are situated in six pairs around the three mutually perpendicular 2-fold axes of the icosahedron.[21] Both Au_{15} and Au_{25} structures are expected to have symmetric gold core structures, which preclude any intense SH generation. The nature of staple motifs protecting the gold core and in particular the structuration of Au-S bonds may be different between Au_{15} and Au_{25} clusters, and may account for enhanced SH signal for Au_{15}.

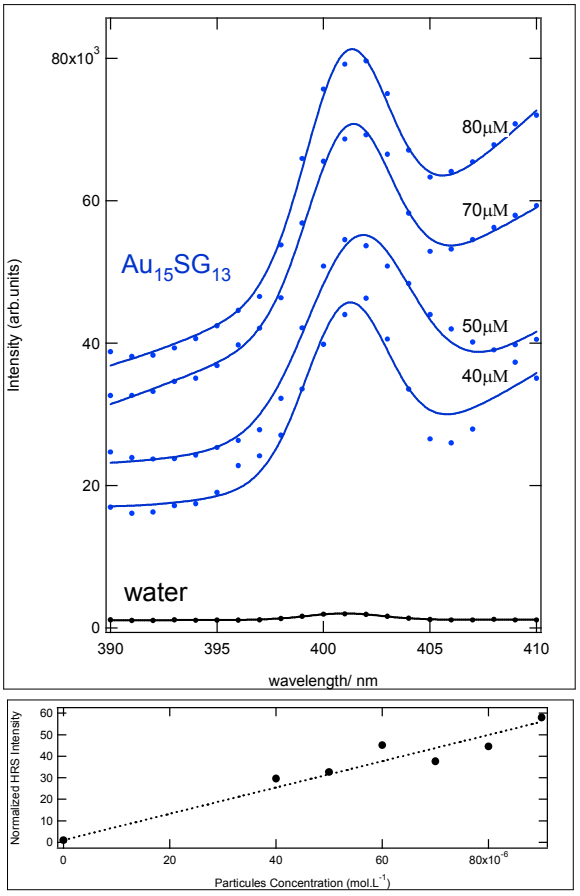

Figure 3: (top panel) HRS intensity versus wavelength for $Au_{15}SG_{13}$ solutions of different concentrations (blue circles). Lines : fit to a Gaussian function superposed on a linearly increasing function of the wavelength. (bottom panel) Plot of the HRS intensity of for $Au_{15}SG_{13}$ as a function of concentration. The continuous lines correspond to the linear adjustment to eq (3).

Also, the 2-photon absorption leads a resonant excitation (around 400 nm). This resonant SH generation is in competition with a vibronic relaxation leading to two-photon emission. Differences in the dynamics of relaxation may also account for the difference of first hyperpolarizability reported for Au_{15} and Au_{25}. Finally, we would like to emphasize that the 10^{30}.β/atom values reported for Au_{15} and Au_{25} clusters are more than two order of magnitude larger than the values reported for Au NPs in the size range 10-50 nm (see Fig. 4 and Table S1 in supporting information). 10^{30}.β/atom values decrease drastically with increasing the number of gold atom and there is a saturation-type of behavior for large gold nanoparticles. The results can be explained by the evolution and involvement of interband transitions in smaller clusters, outlining transition of the cluster behavior to a gold nanoparticle behavior possessing strong surface plasmon absorption.

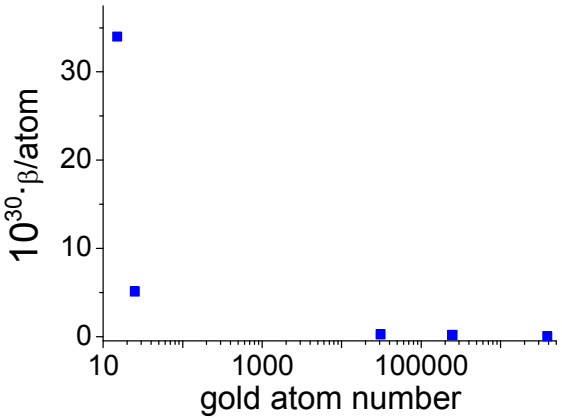

Figure 4: 10^{30}.β/atom as a function of the number of gold atom, obtained with 802 nm excitation.

Solution	10^{30}β (esu) (water=0.087.10^{-30}esu)	10^{30}.β/atom (water=0.087.10^{-30}esu)
$Au_{15}SG_{13}$	509(12)	34
$Au_{25}SG_{18}$	128(1)	5.1
$Au_{25}Cyst_{18}$	163(4)	6.5

Table 1 : Quadratic hyperpolarizabilities for the different solutions at 802 nm.

Conclusions

In summary, size-controlled synthesis of monodispersed gold nanoclusters offers the possibility to address non-linear optical properties of ultrasmall gold quantum clusters in solution. Both the size (Au_{15} and Au_{25}) and the nature of ligands (glutathione vs cysteine) were varied to fathom their influence on the nonlinear behavior of such low nuclearity gold clusters upon two-photon excitation. Au_{15}, the *smallest* stable thiolated gold nanocluster presents remarkable two-photon nonlinear properties. $Au_{15}SG_{13}$ appears to be a good candidate for nonlinear optical microscopies by either two photon microscopy or second harmonic imaging microscopy. The present experimental results provide unique benchmarks for theoretical modeling of NLO properties of such clusters, although the origin of enhanced NLO properties of Au_{15} clusters, as well as the interplay between the cluster core and the interface between ligand shell and the metallic part needs to be clarified. These NLO data are supposed to be highly sensitive to structure of gold clusters and we anticipate that our work could help to unambiguously assign structures for such low nuclearity gold clusters. Works under these lines are currently undertaken in our lab.

Materials and methods

Materials. All the chemicals were commercially available and were used without purification. HAuCl4•3H2O, trifluoroacetic acid (TFA), methanol (HPLC grade), acrylamide (98%), bis-acrylamide (98%), glycine, tris(hydroxymethylamine), cysteine and GSH (γ-Glu-Cys-Gly, MW 307) were purchased from Carl Roth. Sodium borohydride ($NaBH_4$) and tetramethylammonium borohydride ($(CH_3)_4BH_4$) were purchased from Sigma Aldrich. MilliQ water with a resistivity of 18.2 MΩ cm was used for all experiments.

Preparation of protected gold clusters. The detailed synthesis of $Au_{15}SG_{13}$ is available in the supporting information. Briefly, 234 mg of Glutathion (GSH) was dissolved in 35 ml of methanol and 4 ml of tributylamin in a 100 ml balloon. Then 15 ml of ether was added followed by 5ml of a water gold solution (100 mg of $HAuCl_4$,$3H_2O$). Solution was mixed at -10°C during 1 hour and gold salt was reduced by adding tetrabutylammonium borohydride. The solution was kept the night at ambient temperature before being concentrated to a volume of ≈5 ml in a rotary evaporator. The precipitation is induced by adding methanol (5ml) and ether (15ml). Then precipitated was washed to removed unreacted glutathione and unwanted Au_xSG_x.
Protected Au_{25} clusters were synthesizing as described by T. Pradeep and co-workers[15] for $Au_{25}SG_{18}$ and by J. Xie and co-workers[16] for $Au_{25}Cys_{18}$.

Polyacrylamide gel electrophoresis (PAGE). PAGE separation was carried out by using a vertical gel electrophoresis unit with a size of 0.2 cm × 20 cm × 20 cm. The separating and stacking gels were prepared by acrylamide monomers with the total contents of 35 and 7 wt% (acrylamide/bis-(acrylamide) 94:6), respectively. The eluting buffer consisted of 192 mM glycine and 25 mM tris(hydroxymethylamine). The as-prepared Au(SG) clusters were dissolved in a 15% (v/v) glycerol/water solution (6 mg in 100 µl). The samples solutions were loaded onto the stacking gel (10 µl per well) and eluted for 14 h at a constant voltage mode (150 V) to achieve sufficient separation.

Mass spectrometry. Solutions were diluted without gel separation at a concentration of ~1 mg/mL in H2O, electrosprayed at a flow rate of 10 µL/min and analyzed in negative mode with a linear quadruple ion trap mass spectrometer (LTQ, Thermo Fisher Scientific, San Jose, CA) with a spray voltage of −3 kV and a capillary temperature of 100 °C. Other instrument settings were adjusted for each species to optimize the distribution of charge states observed in the mass spectrum. Isotope-resolved mass spectrum were recorded using the ultra zoom scan mode of the instrument (mass resolution ~ 30 000, mass accuracy 0.2 Th).[31] Collision-induced dissociation (CID) was performed using helium gas at a normalized collision energy of 12% for 30 ms.

Absorption and emission measurements. UV−vis spectra in solution were recorded using an AvaSpec-2048 fiber optic spectrometer and an AvaLight-DH-S deuterium halogen light source. Fluorescence excitation and emission spectra were measured using a Fluoromax-4 Horiba fluorescence spectrophotometer.

HRS and TPE measurements. The light source for the present HRS and TPE experiments was a mode-locked femtosecond Ti:sapphire laser delivering at the fundamental wavelength of 800 nm pulses with a duration of about 140 femtoseconds at a repetition rate of 76 MHz. After passing through a low-pass filter to remove any unwanted harmonic light generated prior to the cell, the fundamental beam of about 300 mW was focused by a microscope objective into a 1 cm spectrophotometric cell containing the aqueous solution. The HRS (or TPE) light was collected at an angle of 90° from the incident direction by a 2.5 cm focal length lens. The second harmonic light was separated from its linear counterpart by a high-pass filter and a monochromator positioned on the second harmonic wavelength. The HRS light was then detected with a photomultiplier tube and the pulses produced counted with a photon counter. The fundamental beam was chopped at about 115 Hz to enable a gated photon counting mode allowing automatic subtraction of the noise level. For TPE signal, a short pass filter with a cut-off wavelength at 750 nm was placed before the monochromator to minimize the light scattering from the excitation beam.

Notes and references

Institut Lumière Matière, UMR5306 Université Lyon 1-CNRS,
Université de Lyon 69622 Villeurbanne cedex, France
Fax: +33 4 72 43 15 07; Tel: +33 4 72 43 10 85
rodolphe.antoine@univ-lyon1.fr

Electronic Supplementary Information (ESI) available: Detailed synthesis and purification for $Au_{15}SG_{13}$ clusters. MS and optical spectra for $Au_{25}SG_{18}$ and Au_{25} Cys_{18}. Hyperpolarizability data for gold NPs. Two-photon emission spectra at different pump powers for $Au_{15}SG_{13}$ clusters. Detailed TPA experimental arrangement. See DOI: 10.1039/b000000x/

1. R. C. Jin, *Nanoscale*, 2010, 2, 343-362.
2. P. K. Jain, X. H. Huang, I. H. El-Sayed and M. A. El-Sayed, *Acc. Chem. Res.*, 2008, 41, 1578-1586.
3. S. Link and M. A. El-Sayed, *Int. Rev. Phys. Chem.*, 2000.
4. S. H. Yau, O. Varnavski and T. Goodson, *Acc. Chem. Res.*, 2013, 46, 1506-1516.
5. R. Philip, P. Chantharasupawong, H. Qian, R. Jin and J. Thomas, *Nano Lett.*, 2012, 12, 4661-4667.
6. G. Ramakrishna, O. Varnavski, J. Kim, D. Lee and T. Goodson, *J. Am. Chem. Soc.*, 2008, 130, 5032-5033.
7. L. Polavarapu, M. Manna and Q.-H. Xu, *Nanoscale*, 2011, 3, 429-434.
8. P. N. Prasad, *Introduction to Biophotonics*, Wiley Interscience 2003.
9. L. Moreaux, O. Sandre, S. Charpak, M. Blanchard-Desce and J. Mertz, *Biophys. J.*, 2001, 80, 1568-1574.
10. D. A. Dombeck, M. Blanchard-Desce and W. W. Webb, *J. Neurosci.*, 2004, 24, 999-1003.
11. B. A. Nemet, V. Nikolenko and R. Yuste, *J Biomed Opt.* , 2004, 9, 873-881.
12. Y. Hamanaka, N. Okada, K. Fukagawa, A. Nakamura, Y. Tai and J. Murakami, *J. Phys. Chem. C*, 2012, 116, 10760-10765.
13. S. Kumar, E. S. Shibu, T. Pradeep and A. K. Sood, *Optics Expr.*, 2013, 21, 8483-8492.
14. S. A. Khan, D. Senapati, T. Senapati, P. Bonifassi, Z. Fan, A. K. Singh, A. Neeley, G. Hill and P. C. Ray, *Chem. Phys. Lett.*, 2011, 512, 92-95.
15. E. S. Shibu, M. A. H. Muhammed, T. Tsukuda and T. Pradeep, *J. Phys. Chem. C*, 2008, 112, 12168-12176.
16. Y. Yu, Z. Luo, Y. Yu, J. Y. Lee and J. Xie, *ACS Nano*, 2012, 6, 7920-7927.
17. J. J. Hagen and C. A. Monnig, *Anal. Chem.*, 1994, 66, 1877-1883.
18. F. Lux, A. Mignot, P. Mowat, C. Louis, S. Dufort, C. Bernhard, F. Denat, F. Boschetti, C. Brunet, R. Antoine, P. Dugourd, S. Laurent, L. V. Elst, R. Muller, L. Sancey, V. Josserand, J.-L. Coll, V. Stupar, E. Barbier, C. Rémy, A. Broisat, C. Ghezzi, G. Le Duc, S. Roux, P. Perriat and O. Tillement, *Angew. Chem. Int. Ed.*, 2011, 50, 12299-12303.
19. Y. Negishi, K. Nobusada and T. Tsukuda, *J. Am. Chem. Soc.*, 2005, 127, 5261-5270.
20. Y. Negishi, Y. Takasugi, S. Sato, H. Yao, K. Kimura and T. Tsukuda, *J. Am. Chem. Soc.*, 2004, 126, 6518-6519.
21. M. Zhu, C. M. Aikens, F. J. Hollander, G. C. Schatz and R. Jin, *J. Am. Chem. Soc.*, 2008, 130, 5883-5885.
22. J. Akola, M. Walter, R. L. Whetten, H. Hakkinen and H. Gronbeck, *J. Am. Chem. Soc.*, 2008, 130, 3756-+.
23. Y. Shichibu, Y. Negishi, T. Tsukuda and T. Teranishi, *J. Am. Chem. Soc.*, 2005, 127, 13464-13465.
24. H. Tsunoyama, H. Sakurai, Y. Negishi and T. Tsukuda, *J. Am. Chem. Soc.*, 2005, 127, 9374-9375.
25. C. Xu and W. W. Webb, *J. Opt. Soc.Am. B*, 1996, 13, 481-491.
26. M. A. Albota, C. Xu and W. W. Webb, *Appl. Opt.*, 1998, 37, 7352-7356.
27. J. Duboisset, G. Matar, I. Russier-Antoine, E. Benichou, G. Bachelier, C. Jonin, D. Ficheux, F. Besson and P. F. Brevet, *J. Phys. Chem. B*, 2010, 114, 13861-13865.
28. J. Duboisset, A. Deniset-Besseau, E. Benichou, I. Russier-Antoine, N. Lascoux, C. Jonin, F. Hache, M.-C. Schanne-Klein and P.-F. Brevet, *J. Phys. Chem. B*, 2013, 117, 9877-9881.
29. A. Tlahuice-Flores, M. Jose-Yacaman and R. L. Whetten, *Phys. Chem. Chem. Phys.*, 2013, 15, 19557-19560.

30. D. Jiang, S. H. Overbury and S. Dai, *J. Am. Chem. Soc.*, 2013, 135, 8786-8789.
31. F. Bertorelle, R. Hamouda, D. Rayane, M. Broyer, R. Antoine, P. Dugourd, L. Gell, A. Kulesza, R. Mitric and V. Bonacic-Koutecky, *Nanoscale*, 2013, 5, 5637-5643.